

RSC Advances



This is an *Accepted Manuscript*, which has been through the Royal Society of Chemistry peer review process and has been accepted for publication.

Accepted Manuscripts are published online shortly after acceptance, before technical editing, formatting and proof reading. Using this free service, authors can make their results available to the community, in citable form, before we publish the edited article. This *Accepted Manuscript* will be replaced by the edited, formatted and paginated article as soon as this is available.

You can find more information about *Accepted Manuscripts* in the [Information for Authors](#).

Please note that technical editing may introduce minor changes to the text and/or graphics, which may alter content. The journal's standard [Terms & Conditions](#) and the [Ethical guidelines](#) still apply. In no event shall the Royal Society of Chemistry be held responsible for any errors or omissions in this *Accepted Manuscript* or any consequences arising from the use of any information it contains.

Cite this: DOI: 10.1039/c0xx00000x

www.rsc.org/xxxxxx

ARTICLE

Dynamics study on graphene mediated pyrazinamide drug delivery onto *pncA* protein

Nabanita Saikia,^a Anupam N. Jha^b and Ramesh C. Deka^{*a}

Received (in XXX, XXX) Xth XXXXXXXXX 200X, Accepted Xth XXXXXXXXX 200X

DOI: 10.1039/b000000x

To understand the prospects of graphene nanomaterials in studying complex biomolecular systems, we performed molecular docking and molecular dynamics (MD) simulations on interaction of pyrazinamide (PZA) drug and PZA functionalized graphene with *pncA* enzyme. Docking simulations predict the plausible binding mode of graphene/PZA system with *pncA* protein and advocates that, PZA functionalized onto graphene facilitate in target specific binding of PZA within the protein following a lock and key mechanism. In absence of PZA, graphene exhibits enhanced attractive interaction with adjoining amino acid residues along the binding pathway demonstrating significant extent of rippling within the sheet. The simulations highlight that presence of graphene arrests the free rattling movement of PZA around the binding pocket of protein, thereby improving specificity towards targeting. Interestingly, no major structural deformation in protein was induced by presence of graphene and interaction between ligand and receptor is mainly hydrophobic in nature. The energetics of interaction demonstrates that noncovalent van der Waals and Coulombic forces play the foremost role towards PZA binding with *pncA* protein.

Introduction

The emergence of graphene since its discovery in 2004¹ has catapult tremendous research interest, accounted to its outstanding ballistic transport,² long mean free path at room temperature,³ integral and half integral quantum hall effect,^{4,5} and massless relativistic carriers.⁶ Graphene is considered to be the mother of all graphitic forms, as a single graphene sheet can be rolled to form 0D fullerene, 1D carbon nanotube or stacked to form 3D graphite.⁷ Research targeted towards understanding and exploiting the extraordinary properties of graphene has led to quest in its advanced biomedical research and application namely, in gene delivery,⁸ drug delivery,⁹ biomolecular sensors,¹⁰ cellular imaging,¹¹ and tumor therapy.¹² The modification of graphene surface by covalent and noncovalent functionalization helps in improving biocompatibility, solubility and selectivity.^{13,14} Zhang et al. showed that functionalized graphene is quite biocompatible with reduced toxicity and can be employed for multiple loading of anticancer drug molecules.¹⁵

Just as the treatment of cancer is the rationale of global concern, Tuberculosis (TB) is another leading global cause of death worldwide with an estimated death rate of 2–3 million and around 8 million people getting infected per year.¹⁶ One-fifth of the global TB incidences are accounted in India, with 1.8 million new cases per year.¹⁷ Isoniazid (INH) and pyrazinamide (PZA) constitute as the first line antitubercular prodrugs highly effectual against TB, also recommended by the World Health Organization (WHO).¹⁸ PZA, a prodrug devoid of any significant antibacterial activity, is metabolized to its active form (pyrazoic acid) by the amidase activity of *M. tuberculosis* nicotinamidase/pyrazinamidase (MtPncA) encoded by *pncA* gene.¹⁹⁻²¹ Mutation in PZase coding gene (*pncA*) causes

significant loss in PZase activity along with physiochemical alteration in active metal binding.^{22,23} Gallo et al.²⁴ investigated the role of armchair (5,5) single-wall carbon nanotube (SWCNT) and fullerene as nanovectors for loading and delivery of INH drug, mediated by covalent functionalization approach. Working in similar lines, our previous reported results highlighted the fact that SWCNTs can facilitate loading of antitubercular drug molecules both exohedrally (via covalent and noncovalent functionalization) and endohedrally (through encapsulation), facilitating in multiple drug loading within the nanotubes.²⁵⁻²⁸ In a very recent study, Zuo et al. investigated the adsorption of villin protein onto graphene, CNT and C₆₀ using molecular dynamics (MD) simulation²⁹ and observed that π - π stacking interaction plays a dominant role in binding of protein with graphene which controls the kinetics and thermodynamics of adsorption. Although various experimental studies have aspired towards unraveling the nature governing protein-graphene interactions²⁹⁻³¹ no systematic study has yet come up towards investigating the interaction mechanism of graphene loaded chemotherapeutic drugs with proteins both at experimental and theoretical fronts.

In a way towards confronting the need for advanced drug delivery systems as future avenues in biomedical research, we employ molecular docking and MD simulations to contemplate the role of graphene nanomaterial in PZA binding within active site of *pncA* enzyme. Molecular docking serves as an instrumental tool in computer aided drug design that aims at predicting preferred binding mode of ligand to receptor (mainly protein), which sometimes becomes difficult to comprehend experimentally. Docking studies provide insight into (i) characterization of binding cavity of protein, (ii) orientation of ligand with respect to receptor protein, and (iii) extent of

interaction of protein with functionalized nanomaterial. The molecular docking simulations are based on simulated annealing,^{32,33} tabu search³⁴ and evolutionary algorithms.³⁵ Docking methods are usually determined on the basis of energy scoring functions which represent as mathematical methods widely adopted in drug discovery applications to predict the binding strength or affinity of a ligand to target receptor. Scoring functions help in predicting and classifying correct docked complex from a set of putative ligand binding conformations and ranks the different conformers based on binding mode (relying on energy score values). A lower (more negative) is energy score value signifies better extent of interaction³⁶ that can help in understanding mode of interaction between the two units. The scoring function, as proposed by Gehlharr et al.,³⁷ is derived from piecewise linear potential (PLP), and includes H-bonding and electrostatic terms. For a detailed discussion and understanding on MolDock and energy scoring function used in molecular docking, we would like to suggest reading of the two Refs.^{36,38}

As a follow up of our previous study on dynamics of SWCNT aided PZA drug targeting onto pncA protein³⁹ the present report brings in new insights by demonstrating that graphene can also serve as potential payloads for PZA with observed flexibility towards precise drug targeting. We anticipate that our findings can provide a vivid although qualitative understanding on nature of interactions and how graphene nanomaterial in addition to contemporary SWCNT, can aid in better recognition and facilitate in enhanced PZA orientation within the active site of pncA protein.

30 Computational Details

Molecular docking

The MolDock scoring function (MolDock score, E_{score}) is based on evolutionary algorithm, which combines the differential evolution with cavity prediction algorithm,⁴⁰ given by:

$$E_{\text{score}} = E_{\text{inter}} + E_{\text{intra}} \quad (1)$$

where E_{inter} is the ligand–protein interaction energy:

$$E_{\text{inter}} = \sum_i \sum_j \left[E_{\text{PLP}}(r_{ij}) + 332.0 \frac{q_i q_j}{4r_{ij}^2} \right] \quad (2)$$

The E_{PLP} term is a constituent of two sets of parameters: one for approximating the steric (van der Waals) term between atoms, and another for hydrogen bonds. The second term denotes electrostatic interactions between charged atoms, which is a Coulomb potential with a distance-dependent dielectric constant given by: $D(r) = 4r$. The numerical value of 332.0 fixes the unit of electrostatic energy to kcal/mol.

E_{intra} represents internal energy of ligand given by:

$$E_{\text{intra}} = \sum_i \sum_j E_{\text{PLP}}(r_{ij}) + \sum_{\text{flexiblebonds}} A [1 - \cos(m\theta - \theta_0)] + E_{\text{clash}} \quad (3)$$

where double summation is between all atom pairs in the ligand excluding atom pairs which are connected by two bonds. The second term represents torsional energy, where θ is the corresponding torsional angle. The last term, E_{clash} , assigns a penalty of 1000 if distance between two heavy atoms (more than two bonds apart) is less than 0.2 nm.

To further improve docking accuracy, re-rank scoring function is introduced which identifies the most promising docked conformation from a number of obtained solutions (poses). The re-rank scoring function includes sp^2 – sp^2 torsion, Lennard–Jones (LJ) potential,⁴¹ van der Waals (vdW), electrostatic and solvent interactions.

The prediction of active binding site of mycobacterium PZase was carried out by docking bare PZA with wild type *M. Tuberculosis* pncA protein, the crystal structure retrieved from protein data bank (PDB: 3PL1).¹⁹ To comprehend the means of PZA targeting in presence of graphene, we docked PZA functionalized graphene with pncA in a similar fashion as adopted for PZA/pncA. The docking was performed using Molegro Virtual Docker⁴² for active binding of graphene/PZA onto pncA, which yields an accuracy of around 87 % compared to other available docking tools.⁴³ We conducted 100 independent runs for each of the complex and best docked conformation was selected on the basis of MolDock, re-rank score values and visualized using Molegro Virtual Viewer and Chimera⁴⁴ packages. The simplex evolution (SE), population size, maximum interactions, energy threshold, and crossover rate values were set to 300, 50, 1000, 100 and 0.90, respectively.

MD simulation

Five set of systems were considered for MD simulation: (1) pncA/PZA, (2) pncA/graphene, (3) pncA/PZA functionalized graphene, (4) graphene without PZA and (5) PZA/graphene without pncA. The simulations were performed using Gromacs package 4.5.0 with OPLS-AA force field.⁴⁵ A model 6×6 graphene flake was considered for the dynamics study having dimension of 1.664 nm × 1.664 nm, and optimized geometries of PZA and 6×6 graphene are depicted in Supporting Information, Fig. S1. The force field parameters for carbon and hydrogen atoms of simulated graphene flake are provided in Supporting Information, Table S1. In the initial conformation, graphene and pncA was well separated, at a distance of ~ 2.0 nm, measured from the active site (binding pocket) of pncA and graphitic basal plane. The combined systems, placed in a cubic periodic supercell was then solvated using TIP3P water model, where distance between solute molecules (here, water is considered as solvation medium) and box boundary was maintained around 1.5 nm. The distance criterion for long-range electrostatic interaction (particle–mesh Ewald (PME) method) and vdW interaction was set at 0.12 and 1.0 nm, respectively. The energy minimization was followed by equilibration for 1 ns at constant pressure (1 bar) and temperature (298 K) using the Berendsen coupling.⁴⁶ The dynamics run of 40 ns in case of systems (1–3) in an NVT ensemble at 298 K was performed for better correlation of observed trends and ensure reproducibility of our findings. Although current MD simulations are being reported for much longer time scales, due to our computational limitation, we have restricted to 40 ns, although nevertheless, we do not compromise in consistency of the reported results. In addition, we performed 10 ns simulation for systems (4) and (5) to correlate the influence of pncA towards observed rippling of small graphene flake considered. The visualization of snapshots and trajectories at

different time frames during the course of dynamics simulation was projected using VMD⁴⁷ and PyMOL⁴⁸ packages to get a pictorial depiction of the interaction. The MD trajectory file for the studied systems were used to extract the dynamical 5 observables (snapshots) at different time spans, discussed in detail in subsequent sections.

Angle deficit parameter as a measure of curvature in graphene⁴⁹

10 In planar graphene, bond angle between carbon atom and nearest neighbor is calculated as 120°. The rippling of graphene introduces an induced curvature, thereby deflecting the bond angle from normal 120°. The localized perturbation in planarity of finite 6×6 graphene flake, deduced using the vertex angle deficit (δ_v) parameter is given by:

$$\delta_v = (\text{Sum of nearest neighbor angles of curved configuration, } n) - (\text{Sum of the angles of planar graphene})$$

$$\delta_v = n - 360^\circ \quad (4)$$

The δ_v parameter helps in quantifying extent of curvature of 20 graphene at localized sites and average over multiple configurations yield the precise value of curvature angle. We calculated the extent of curvature in graphene during the course of simulation with and without *pncA* using the δ_v parameter on specific C atom site exhibiting maximum degree of rippling 25 during the simulation.

Energy parameters

To investigate the energetics of interaction of perfect and functionalized graphene with *pncA* protein, we compared the 30 different energy components namely, total energy, potential energy and the non-bonded energy (mainly vdW and Coulomb forces) for the five sets of system. In general, total energy of system is described as a sum of the following terms⁵⁰

$$E_{\text{total}} = E_{\text{valence}} + E_{\text{cross-term}} + E_{\text{nonbonded}} \quad (5)$$

where E_{valence} term is further split into:

$$E_{\text{valence}} = E_{\text{bond}} + E_{\text{angle}} + E_{\text{torsion}} + E_{\text{oop}} + E_{\text{UB}} \quad (6)$$

Although the first four terms are self explanatory, Urey–Bradley (UB) term involves interactions between two atoms that are connected by a common atom. $E_{\text{cross-term}}$ involves mixing of 40 bond stretch, angle bending and torsional interactions.

The non-bonded energy, $E_{\text{nonbonded}}$ is defined by:

$$E_{\text{nonbonded}} = E_{\text{vdW}} + E_{\text{Coulomb}} + E_{\text{H-bond}} \quad (7)$$

where $E_{\text{vdW}} + E_{\text{Coulomb}} + E_{\text{H-bond}}$ denote vdW, Coulombic and H-bonded energy terms, respectively.

Results and discussion

Docking of PZA/graphene with *pncA* protein

Scorpio and Zhang in 1996 identified the PZase gene (*pncA*) from *M. tuberculosis* and showed that mutation in *pncA* forms the major mechanism towards PZA resistance.²¹ The crystal structure of *pncA*, as illustrated in Fig. 1, comprises of six stranded parallel beta sheet with helices packed on either side to form a α/β domain.⁵¹ The active binding residues namely, Asp49, His51, His57, His71 and Cys138 are labelled in closest proximity to binding pocket for PZA interaction and drug activation (Fig. 1). The His51, His57, and Asp49 residues serve as Fe^{2+} binding site;

whereas, Asp8, Lys96, and Ser104 residues function as catalytic centre located in close proximity to Cys138 (which is the putative active site).⁵² For a vivid description of binding site within *pncA* 60 protein, the figure directed by arrow on to the right provide an illustration of binding region, with mesh area corresponding to the binding pocket onto which PZA needs to get docked. The Fe^{2+} ion is coordinated to His51, His71 residues; HOH220, HOH221 water molecules (represented by red dots) form a 65 tetragonal bipyramidal structure with H_2O molecules lying at the equatorial position and side chain residues (Asp49 and His57) occupy the axial positions.

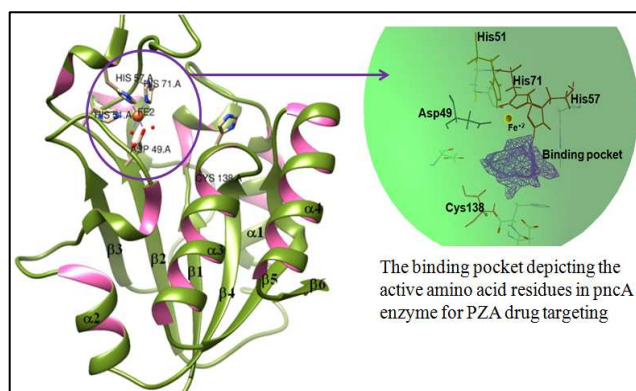


Fig. 1. The optimized structure of *pncA* depicting active binding site (blue circle), and zoom in of the binding pocket (shown in 70 mesh region) with the highlighted active amino acid residues.

The docking of bare PZA with *pncA* has been discussed in detail in our previous study.⁵³ The docking of PZA functionalized graphene with *pncA* (Fig. 2a and b) illustrates PZA to get grooved 75 within the binding pocket and graphene remains in close proximity along the entering pathway.

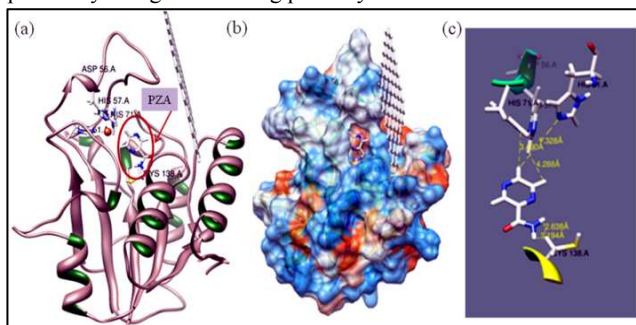


Fig. 2. The docked conformation of (a) *pncA* with PZA functionalized 6×6 graphene, (b) corresponding hydrophobic surface, (c) optimum interacting distance of PZA with closely 80 oriented amino acid residues.

The electrostatic surface plot (Fig. 2b) depicts PZA to remain within active region with graphene situated close to the entering pathway, restrained by the dimension of the sheet. The presence 85 of graphene does not affect overall protein conformation during docking (Fig. 2a and b), nor does it gets plugged within protein, in which case, it may lead to severe perturbation in protein physiological properties. The interacting distance between PZA and closely situated Cys138 residue in PZA–graphene/*pncA*

system is calculated as 0.264 nm and for PZA/pncA system distance between PZA and Cys138 residue is 0.278 nm and 0.354 nm with His57 residue (Fig. 2c). The presence of graphene thereby aids in improved PZA binding with selective amino acid residues of *pncA*. The docking of bare PZA demonstrates a MolDock score of -54.644 (arbitrary units) and re-rank score value of -46.609 (arbitrary units).⁵³ Upon functionalization of PZA with graphene and subsequently docking with *pncA*, MolDock and re-rank scores increase to -56.054 and -47.553 (arbitrary units), respectively suggesting that presence of graphene facilitates in enhanced PZA binding onto the active site of *pncA* with improved energy score values and decreasing interacting distance.

15 Simulation of PZA, graphene and PZA functionalized graphene with pncA

MD simulations of graphene/*pncA*, PZA/*pncA* and PZA-graphene/*pncA* was performed to further substantiate the docking results; get a definitive insight towards the course of PZA drug trafficking in the vicinity of protein and exemplify the role of graphene in PZA drug delivery. The simulation results are discussed in detail in subsequent sub-sections.

Simulation of perfect graphene with pncA protein

Fig. 3 depicts the snapshots at different time frames (extracted from MD trajectories) corresponding to simulation of 6×6 graphene with *pncA* in absence of PZA. At 0 ns, graphene encloses the binding cavity of *pncA* lying within the non-interacting distance with respect to proximate amino acid residues. Around 2 ns, the deviation from planarity is observed and graphene reorients and tries to penetrate the binding pathway. As simulation progresses, graphene displays strong potency to remain along the functional pathway and interact with terminal amino acid residues. Although significant fluctuation and subsequent crumpling in graphene conformation was observed throughout the 40 ns simulation time, no major structural deformation in *pncA* was noticed. This shows that perfect

75

graphene (flake) is quite flexible in nature (as we did not constrain the carbon and hydrogen atoms in graphene) and undergoes non-bonded interactions with adjoining amino acid residues of *pncA*.

The graphene flake was isolated from the simulation snapshots and extent of curvature was calculated with vertex angle deficit (δ_v) parameter as defined in Eq. 4. Although we do not have a direct in-hand comparison of bending rigidity and extent of flexibility of model graphene flake considered in our study with reported experimental values,^{49,54} it is noteworthy to mention that calculated vertex angle deficit parameter at 298 K during the simulation supports the elastic behaviour of graphene sheet. The δ_v value for graphene in presence of *pncA* varies in the range of -0.118^0 to -5.524^0 (maximum deflection). The highest deviation in graphene planarity is contributed from terminal edges and inner basal plane exhibits minimum deviation, suggesting conformational flexibility of graphene terminal edges towards the interaction. High degree of crumpling of graphene was observed at simulation time of 7, 15–25 ns and further at 35 and 38 ns, respectively illustrating the high degree of flexibility of small graphene flake.

The root mean square deviation (RMSD) of 6×6 graphene, *pncA* and *pncA*/6×6 graphene combined as depicted in Fig. 4 illustrate RMSD of *pncA* to remain uniform throughout the simulation at an average value of 0.045 nm and suggests no major fluctuations in secondary structure of protein in presence of graphene. Although graphene exhibits random crumpling throughout the simulation time, RMSD keeps fluctuating at an average value of 0.075 nm. In combined system, between 0–2 ns, RMSD drops drastically from ~ 0.39 nm to ~ 0.13 nm, which may be contributed to sudden flip in orientation of graphene around the protein entering pathway. Beyond 2 ns onwards till 40 ns, RMSD remains more or less uniform at an average value of ~ 0.10 nm. Thus, RMSD of 6×6 graphene/*pncA* combined follows a similar trend in the latter half of simulation and major contribution in deviation is from graphene sheet rather than protein.

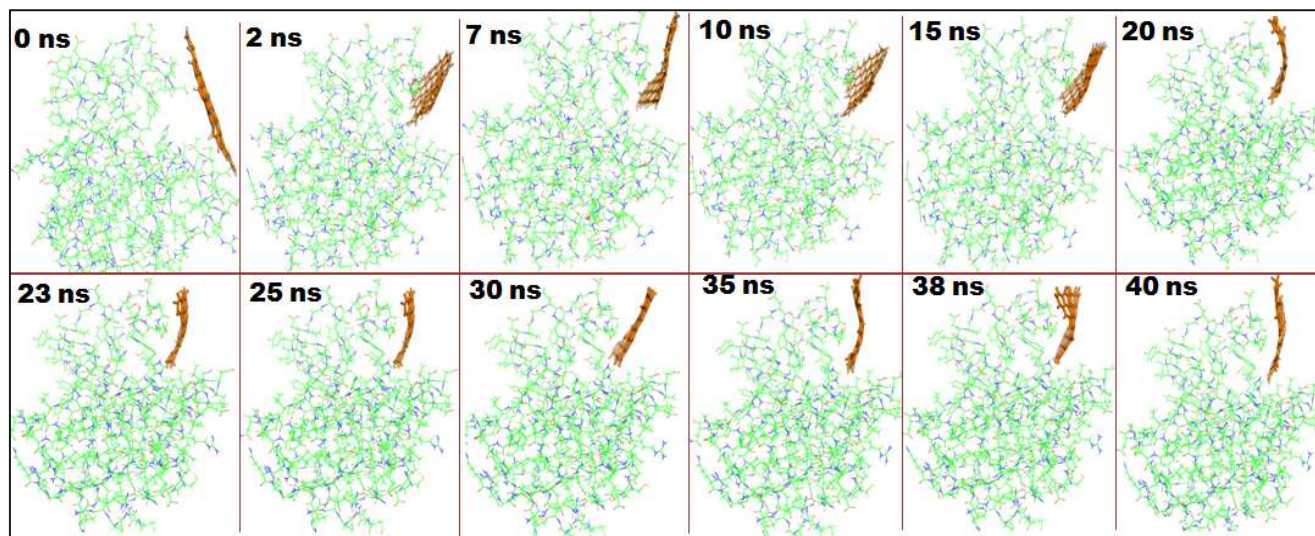


Fig. 3 Representative snapshots corresponding to interaction of 6×6 graphene with *pncA* protein for 40 ns simulation time.

Cite this: DOI: 10.1039/c0xx00000x

www.rsc.org/xxxxxx

ARTICLE

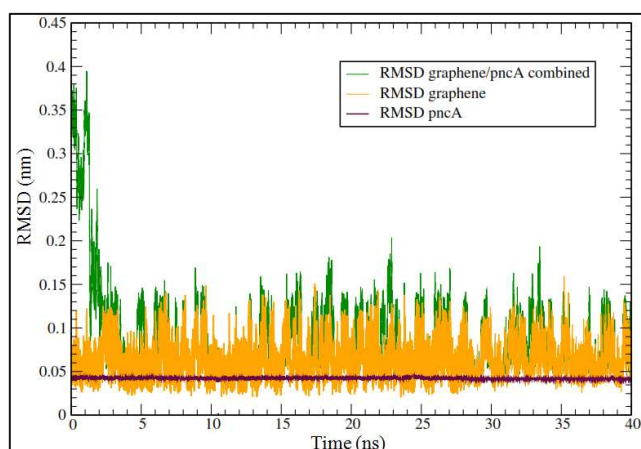


Fig. 4 The RMSD vs. time (ns) for 6×6 graphene, pncA and 6×6 graphene/pncA combined.

Supporting Information, Fig. S2 depicts the interaction of 5 graphene with selected amino acid residues namely Leu19, Ala20, Thr61, Asp63, Tyr64, Ser65, Trp68, His137 and Val163, oriented in close proximity to graphene and Fig. S3a illustrates a comparison of centre of mass (COM) distance between graphene and the selected residues. The distance between graphene–Ser65 10 and graphene–Asp63 is calculated around 0.045 and 0.075 nm, which portray as the closest interacting residues. The distance for other residues fall within the range of weak interaction criteria (< 2 nm). It is quite likely for graphene to exhibit weak noncovalent, H-bonded and π - π stacking interactions with the selected amino 15 acid residues. The hydrophobic effect also plays a crucial role in association of a protein with ligand as hydrophobicity fosters the removal of water and interaction between ligand and receptor.

The root mean square fluctuation (RMSF) of pncA demonstrates significant fluctuations throughout the simulation 20 for most of the protein atoms although overall RMSF varies between 0.020–0.035 nm (Fig. S3b, Supporting Information). These fluctuations can be accounted to possible interaction of the amino acid residues of pncA with graphene during simulation.

25 *Simulation of PZA/pncA in absence of graphene*

We investigated the interaction between pncA protein and PZA in absence of graphene by performing 40 ns simulation. The course of interaction of PZA with pncA was investigated considering three propositions: (1) PZA well separated from 30 protein with respect to COM distance from binding pocket at an initial distance > 2.0 nm,³⁹ (2) PZA placed directly along the entering pathway in near proximity to binding cavity, and (3) PZA docked onto binding pocket of pncA, as illustrated in Fig. 1, right panel. We lay particular emphasis on cases (2) and (3) in 35 this manuscript, because of the propensity towards better binding of PZA with pncA when placed along binding pathway and behavior of PZA in a confined environment. Fig. 5 tracks the dynamics corresponding to selected frames for instance (2), defined for 40 ns. With progress in simulation time, PZA assumes 40 different orientations along the entering pathway, but under no circumstance is it able to overcome the energy barrier and traffic inside the binding pocket of pncA on its own as was observed in case of molecular docking studies. The residues Try68, His137 and Val163, which act as the gatekeeper amino acids prevent ease 45 in PZA passage inside the active region, thereby blocking PZA from trafficking into the active catalytic site.

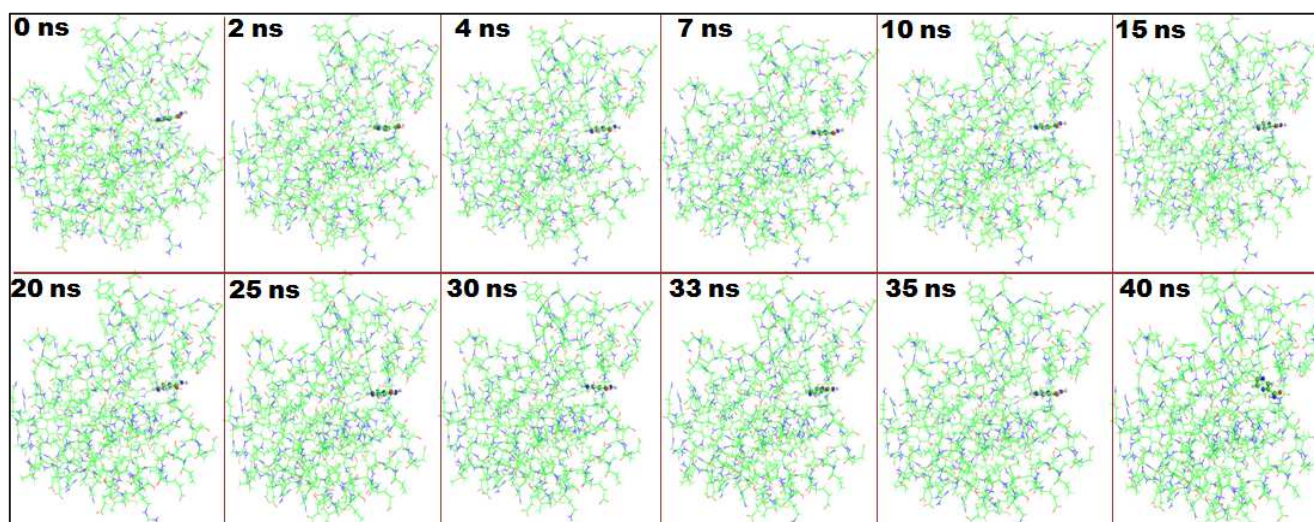


Fig. 5. Representative snapshots corresponding to interaction of bare PZA drug with pncA protein for 40 ns simulation time, with PZA placed along the entering pathway. The frames that gave the major inference with respect to fluctuations in PZA conformation during simulation with pncA are depicted in the figure.

Cite this: DOI: 10.1039/c0xx00000x

www.rsc.org/xxxxxx

ARTICLE

However, unlike our previous reported study on simulation of PZA/pncA system corresponding to instance (1), where we did observe PZA to leave the active region and keep fluctuating in close vicinity of protein, thereby losing its specificity towards interaction, a slightly well defined course for PZA trafficking along pncA (as in case 2) arrests the random fluctuations and secures PZA close to protein. However, it is feasible to obtain the targeted delivery when PZA is loaded or rather functionalized onto carrier payloads like graphene as it facilitates in pronounced interaction between PZA and pncA.

The RMSD of PZA as depicted in Fig. S4a of Supporting Information varies between 0.01–0.03 nm, whereas average RMSD of pncA and PZA/pncA combined is obtained around 0.038 nm suggesting major contribution to RMSD is from the adsorbed PZA molecule which brings in major fluctuations in RMSD values throughout the simulation.

The COM distance of some of selective amino acid residues in close proximity to PZA is depicted in Fig. S4b, Supporting Information. The COM distance falls within 1.0 nm, suggesting favorable interaction of PZA along the binding pathway. Phe13, His137, Leu19 and Val163 exhibits the strongest interactions with PZA (within the range of 0.5–0.6 nm) compared to the other residues and portrays as closely placed residues. Although PZA continuously keeps flipping in close vicinity of pncA, overall, average COM distance values remain more or less uniform for each of the individual amino acids.

In case of scenario (3), simulation snapshots of which are depicted in Fig. S5 of Supporting Information, PZA keeps rattling inside the catalytic active site (binding pocket) showing no potency to come out, which is hindered by thermodynamic favorability towards encapsulated state within the confined space inside pncA. The variation in RMSD for docked conformation demonstrate prominent fluctuations for PZA around 0.01–0.03 nm, compared to RMSD of pncA (~ 0.038 nm) and combined system (0.04 nm) which may be due to random fluctuation in position of less bulky PZA molecule compared to robust pncA within a confined environment (Fig. S6, Supporting Information). The nearest interacting distance between PZA and closely proximate amino acid residues namely Asp8, Phe13, Asp49, His51, His57, His71, Gly97, Thr100, Gly101, Ser104, and Cys138 calculated in the docked conformation is depicted in Fig. 6. The average COM distance lies between 0.5–1.2 nm, suggesting PZA to preferentially undergo strong interactions with these residues. The distance between Cys138–PZA is found to be the least at an average value of 0.55 nm, illustrating the fact PZA interacts strongly with Cys138 within the catalytic active region of pncA. Thus, except in case (3), for the first two sets of simulation, PZA by itself cannot penetrate the active catalytic region, which holds for an extended simulation time as well, but under suitable physiological circumstances, or incorporation of pulling forces (e.g. using steered MD, (SMD) calculations) these

aspects may be addressed to get better insight into the extent and energetics of interaction.

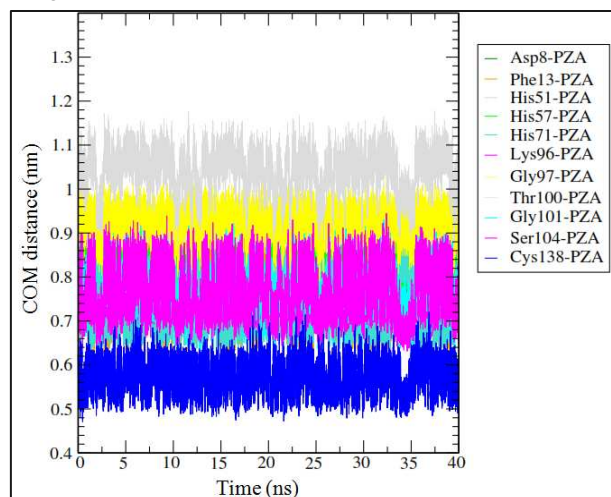


Fig. 6. The variation in COM distance (nm) between PZA and selected amino acid residues of pncA with respect to time (ns) corresponding to PZA docked inside pncA.

Simulation of PZA functionalized graphene with pncA

The representative snapshot for simulation of PZA/6×6 graphene in presence of pncA is illustrated in Fig. 7. Compared to simulation of PZA/pncA, presence of graphene restricts the random rattling of PZA by directing it specifically along the binding cavity. It is quite likely that graphene can assist PZA towards remaining confined mainly in the binding pocket (as observed from docking studies) under suitable physiological conditions. At 0 ns, both graphene and PZA are well separated from protein, with graphene assuming an almost planar conformation. With progress in simulation time, PZA reorients itself in a way that can facilitate in better interaction with adjoining amino acid residues along the entering pathway demonstrating random conformational changes. The presence of graphene, on the other hand, hinders PZA drug from leaving the active region thereby enhancing the interaction of PZA with adjoining amino acid residues. During the simulation, although considerable crumpling of graphene is noticed, quite distinct for snapshots at 2, 10, 12, 15, 30, 35 and 40 ns, graphene however does not penetrate the binding cavity of pncA as was observed in Fig. 3, as it is partially blocked by presence of PZA illustrating that PZA hinders the direct interaction between graphene and terminal amino acid residues of pncA along the entering pathway. At the same time, PZA demonstrates propensity to cooperatively interact with both graphene and protein mediated by the weak noncovalent vdW interactions.

Cite this: DOI: 10.1039/c0xx00000x

www.rsc.org/xxxxxx

ARTICLE

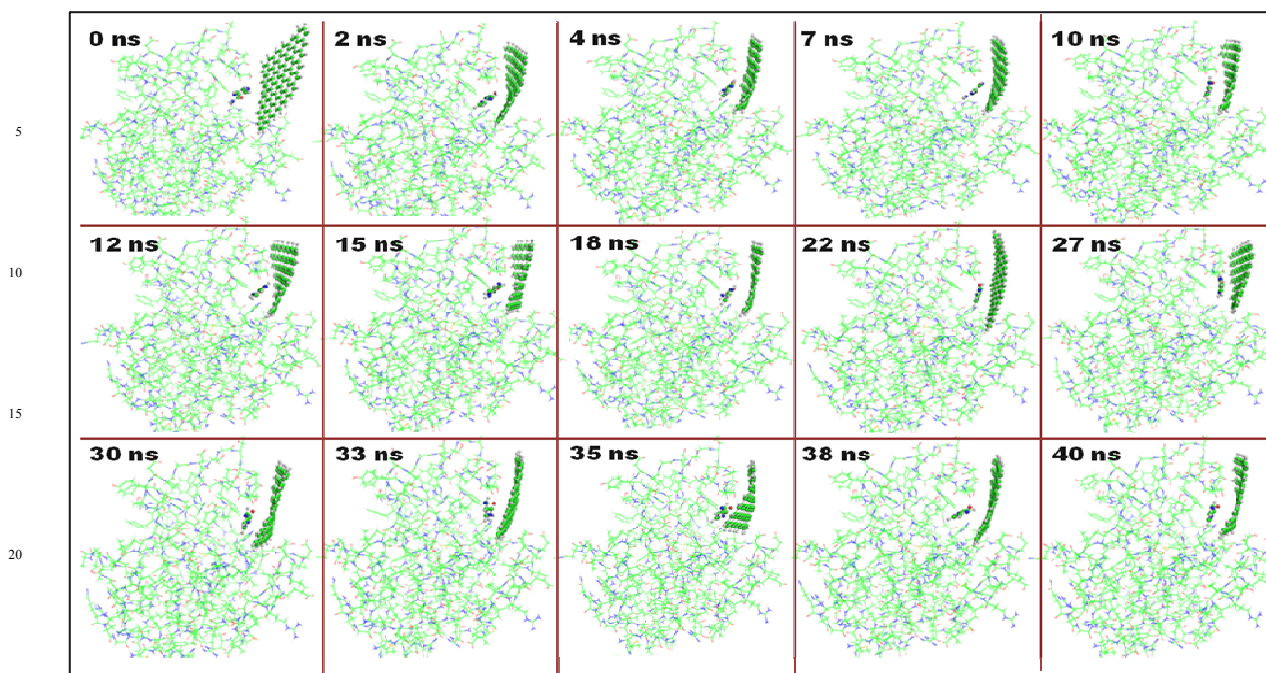


Fig. 7. Representative snapshots corresponding to simulation of PZA/6×6 graphene with pncA for 40 ns. The snapshots that gave the major inference with respect to fluctuations in graphene and PZA conformation during simulation with pncA are depicted in the figure.

The RMSD plot (Fig. 8) illustrate that pncA does not show any major structural changes as inferred from the simulation snapshots at an average value of 0.04 nm similar to that observed in graphene/pncA system.

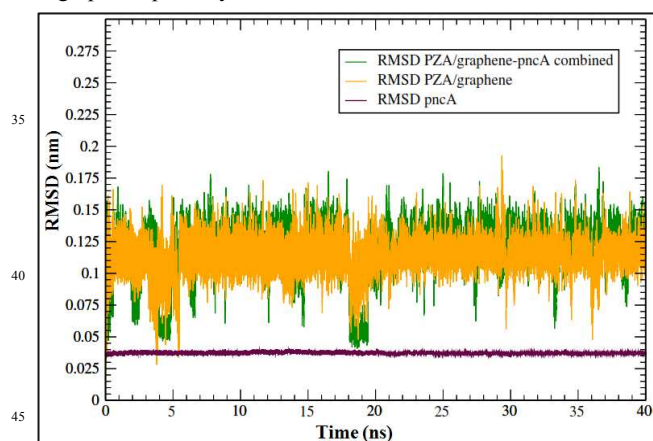


Fig. 8. The RMSD vs. time (ns) plot for 6×6 graphene/PZA, pncA and 6×6 graphene/PZA-pncA combined.

Graphene however exhibits structural fluctuation rendered from its flexible nature with average RMSD value ranging between 0.10–0.135 nm. The RMSD for combined system is obtained at almost comparable value (~ 0.145 nm) to that of graphene with sudden dip in RMSD value around 4 ns and 18–20

ns which is contributed to fluctuations in structural conformations of the ligand rather than protein.

PZA and 6×6 graphene interacts with Asp63, Tyr64, Ser65, Try68, Tyr103, His137, Arg140, Val163, and Thr167 residues positioned along the entering pathway (Supporting Information, Fig. S7a) and variation in COM distance between these residues and PZA/graphene system is depicted in Fig. 9.

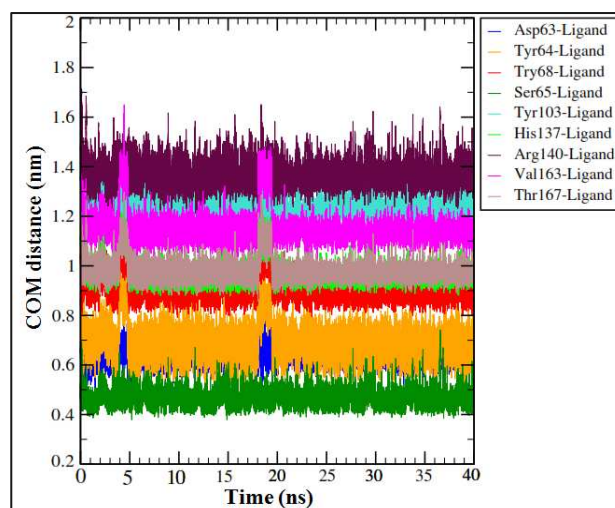


Fig. 9. The variation in COM distances corresponding to simulation of PZA/graphene with pncA protein.

The residues Ser65, Asp63 and Tyr64 are at a closest interacting distance from the ligand at 0.50, 0.65 and 0.75 nm, respectively. Thus, these residues might play a pivotal role in binding of ligand with protein, and the other residues along the entering pathway supposedly participate in PZA trafficking.

The RMSF of pncA (Supporting Information, Fig. S7b) supports the observation from RMSD and overall pncA conformation does not change during simulation. The average RMSF value is obtained around 0.02–0.025 nm, along with fluctuations in some of protein atoms which can be accounted to weak noncovalent interaction between the interacting groups.

Similar to that of perfect graphene, we calculated the extent of curvature of graphene sheet (extracted from PZA/graphene system) using δ_v parameter. The vertex angle deficit value for graphene in PZA/graphene system varies in the range of -0.444° to -1.473° , indicating that extent of deviation from planarity is comparatively lower than perfect graphene, which is further supported from the dynamics snapshots. This suggests that presence of PZA prevents the high degree of crumpling observed in free graphene, thereby imparting structural rigidity and less conformational distortions.

Simulation of graphene and PZA functionalized graphene in absence of pncA

To exemplify the involvement of pncA towards observed flexibility of graphene, we performed 10 ns simulation of graphene and PZA functionalized graphene without pncA protein as depicted in Fig. 10. Free standing graphene in absence of PZA and without the influence of pncA, exhibit significant rippling of the sheet (Fig. 10a–e). The hydrogen terminated edges of graphene are found to be more flexible compared to inner benzenoid rings of basal plane. On adsorption of PZA, dynamic snapshots illustrate the preferentiality for PZA to remain adhered to graphene surface (Fig. 10f–k) mediated by weak noncovalent π - π stacking interaction between the pyrazine ring of PZA and benzenoid rings of graphene, and throughout the simulation, major changes observed are in the associated rippling of graphene. The individual simulations of graphene with and without pncA illustrate that noncovalent functionalization of

small aromatic molecules (in our case PZA) somewhat renders stability towards the observed high crumpling of graphene and rippling is of less order in magnitude compared to simulations in pristine form. Although our investigations are based on a model 6×6 graphene flake, the case may vary for nanosheets with varying dimension, as larger graphene sheets may impose higher extent of flexibility towards the interaction.

Energetics of interaction of PZA functionalized graphene with pncA

To further understand the energetic of interaction of studied sets of systems, we computed the different energy components as summarized in Table 1. The average values of energy components are found to be very high and can be accounted to large system size. From difference in energy values we found that change in total energy of system, is mainly dependent on potential energy parameter rather than kinetic energy. The variation in total and potential energy follows the order:

$$\text{PZA/pncA (docked conformation)} < \text{PZA/pncA (binding pathway)} < \text{graphene/pncA} < \text{PZA-graphene/pncA}$$

(Total energy)

$$\text{PZA-graphene/pncA} < \text{PZA/pncA (docked conformation)} < \text{Graphene/pncA} < \text{PZA/pncA (binding pathway)}$$

(Potential energy)

For graphene/pncA and PZA-graphene/pncA, potential energy for latter is lower than former and this decrease in potential energy value enhances the overall stability of PZA-graphene/pncA system. However, for PZA/pncA systems, potential energy value corresponding to docked conformation is ~ fivefold lower than PZA placed along binding pathway indicating that docked PZA assumes a more energetically favorable state within binding pocket thereby stabilizing the system on the whole. The comparatively high potential energy for PZA/pncA system maybe also due to observed random rattling in position of PZA along the vicinity of protein throughout the simulation and after functionalization with graphene; potential energy value decreases as graphene arrests the free labile movement of PZA.

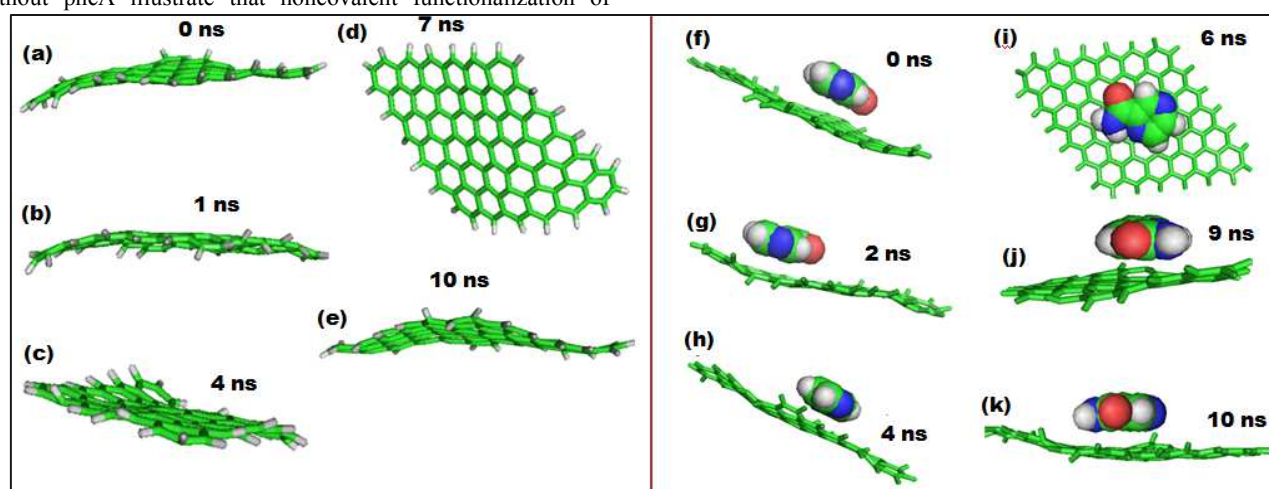


Fig. 10. The snapshots corresponding to simulation of perfect graphene without PZA and pncA protein (a–e), simulation of PZA/graphene without pncA protein (f–k) for 10 ns simulation time.

Cite this: DOI: 10.1039/c0xx00000x

www.rsc.org/xxxxxx

ARTICLE

Table 1. The energy parameters (average energy and difference in energy between initial and final structures) for the studied systems calculated at 298 K temperature. All energy values are in kJ/mol.

System	PZA/graphene-pncA	Graphene/pncA	PZA/pncA (docked conformation)	PZA/pncA (binding pathway)
Total energy (average)	-711842.0	-593289.0	-623580.0	-712610.0
Total energy (difference)	-429.875	-412.50	-773.187	-764.375
Potential energy (average)	-875564.0	-729527.0	-759730.0	-848914.0
Potential energy (difference)	-312.375	-121.187	-266.50	-50.187
Kinetic energy (average)	163722.0	136238.0	136150.0	136304.0
Kinetic energy (difference)	-117.453	-291.297	-506.734	-714.562
vdW energy (average)	123137.0	100381.0	118675.0	150907.0
vdW energy (difference)	-2279.758	-388.867	-672.640	-1426.671
Coulomb energy (average)	-913040.0	-756395.0	-806639.0	-923336.0
Coulomb energy (difference)	-2643.687	-683.875	-428.187	-1737.625

From the non-bonded energy terms (i.e. computed short range (SR) vdW and Coulomb energy), both the energy components play a significant role, however, change in non-bonded energy parameters are much higher for PZA-graphene/pncA system suggesting that presence of graphene nanomaterial facilitates in enhanced stability and better interaction with pncA during the dynamics run. The non-bonded energy terms essentially contribute towards the observed stability of system within a solvated media and follow the order:

PZA-graphene/pncA < PZA/pncA (along binding pathway) < graphene/pncA < PZA/pncA (docked conformation)

Overall, for PZA-graphene/pncA system, noncovalent vdW and Coulombic parameters influence interaction of ligand with protein, and with increase in system size, potential as well as vdW energy value decreases suggesting the enhanced favorability towards ligand binding with pncA protein.

Conclusions

Docking of PZA with pncA protein depicts PZA to get grooved within the active catalytic site of pncA. However, presence of graphene does not induce any major structural deformation or conformational change in protein, which is further supported from MD simulations. During the course of dynamics run for graphene and PZA/graphene systems, graphene sheet remains close to the functional site of pncA and reveals significant non-bonded interactions with adjoining amino acid

residues in close proximity along the entering pathway. The RMSD demonstrate graphene to be more dynamic than robust pncA towards PZA binding thereby restricting free labile rattling of PZA around pncA. The vertex angle deficit parameter illustrates the extent of flexibility of small graphene flake considered in our study. The energetics parameter displays the involvement of noncovalent interactions towards observed stability of system. A detailed understanding on energetics of interaction of ligand with protein can be of profound interest especially from drug delivery perspective. Understanding the forces involved in binding of ligand with target protein can be quite instrumental and forces that govern these interactions are mainly H-bonding, hydrophobic, electrostatic and vdW.

The present study thus provides a qualitative yet succinct understanding on role of graphene nanomaterial in PZA drug interaction with pncA protein that can also facilitate in better drug targeting in contrary to our previous report on SWCNT carrier payload. The simulations although modeled for a small graphene flake, can however serve as guidelines for other graphene based nanomaterials as well of varying dimension. Incorporation of SMD calculations can provide valid definitive interpretation to free energy of binding of ligand to protein which will be our future endeavor and serve towards providing a connecting link between instances (2) and (3) for simulation of PZA and PZA/graphene with pncA protein. We expect that future study in this direction will be quite helpful from drug delivery perspective

to address a broader outlook which will make the study conducive and conclusive enough.

Acknowledgements

NS acknowledges The Council of Scientific and Industrial Research (CSIR), New Delhi, India for the Senior Research Fellowship (SRF). The project is funded by the Department of Science and Technology (DST), New Delhi, India.

Notes and references

^aDepartment of Chemical Sciences, Tezpur University, Napaam, Tezpur-784028, Assam, India. Fax: +91 3712 267005/6;

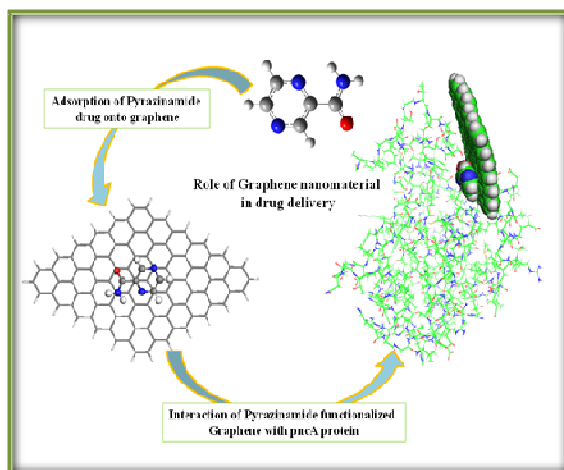
^bDepartment of Molecular Biology and Biotechnology (MBBT), Tezpur University, Tezpur-784028, Assam, India.

E-mail: ramesh@tezu.ernet.in

† Electronic Supplementary Information (ESI) available: The force field parameters for carbon and hydrogen atoms of graphene, simulations snapshots, RMSD and COM variation plots for PZA/pncA system, RMSF plots for graphene/pncA and PZA-graphene/pncA. See DOI: 10.1039/b000000x/ for further details.

References

- K. S. Novoselov, A. K. Geim, S. V. Morozov, D. Jiang, Y. Zhang, S. V. Dubonos, *Science*, 2004, **306**, 666.
- D. Gunlycke, H. M. Lawler, C. T. White, *Phys Rev B*, 2007, **75**, 085418.
- K. S. Novoselov, Z. Jiang, Y. Zhang, S. V. Morozov, H. L. Stormer, U. Zeitler, J. C. Maan, G. S. Boebinger, P. Kim, A. K. Geim, *Science*, 2007, **315**, 1379.
- Y. Zhang, Y.-W. Tan, H. L. Stormer, P. Kim, *Nature*, 2005, **438**, 201.
- K. I. Bolotin, K. J. Sikes, Z. Jiang, M. Klima, G. Fudenberg, J. Hone, P. Kim, H.L. Stormer, *Solid State Commun.*, 2008, 146, 351.
- K. S. Novoselov, A. K. Geim, S. V. Morozov, D. Jiang, M. I. Katsnelson, I. V. Grigorieva, S. V. Dubonos, A. A. Firsov, *Nature*, 2005, **438**, 197.
- A. K. Geim, K. S. Novoselov, *Nat. Mater.*, 2007, **6**, 183.
- N. L. Rosi, D. A. Giljohann, C. S. Thaxton, A. K. R. Lytton-Jean, M. S. Han, C. A. Mirkin, *Science*, 2006, **312**, 1027.
- H. Chen, M. B. Muller, K. J. Gilmore, G. G. Wallace, D. Li, *Adv. Mater.*, 2008, **20**, 3557.
- Y. Liu, D. Yu, C. Zeng, Z. Miao, L. Dai, *Langmuir*, 2010, **26**, 6158.
- X. Michalet, F. F. Pinaud, L. A. Bentolila, J. M. Tsay, S. Doose, J. J. Li, G. Sundaresan, A. M. Wu, S. S. Gambhir, S. Weiss, *Science*, 2005, **307**, 538.
- Z. Liu, J. T. Robinson, X. M. Sun, H. J. Dai, *J. Am. Chem. Soc.*, 2008, **130**, 10876.
- S. Niyogi, E. Bekyarova, M. E. Itkis, J. L. McWilliams, M. A. Hamon, R. C. Haddon, *J. Am. Chem. Soc.*, 2006, **128**, 7720.
- J. R. Lomeda, C. D. Doyle, D. V. Kosynkin, W. F. Hwang, J. M. Tour, *J. Am. Chem. Soc.*, 2008, **130**, 16201.
- L. Zhang, J. Xia, Q. Zhao, L. Liu, Z. Zhang, *Small*, 2010, **6**, 537.
- S. T. Cole, K. D. Eisenach, D. N. McMurray, W. R. Jacobs Jr. (eds.): *Tuberculosis and the tubercle bacillus*. ASM Press, Washington, 2005.
- M. Vasantha, P. G. Gopi and R. Subraman, *Indian J. Tuberc.*, 2008, **55**, 64.
- D. Maher, P. Chaulet, S. Spinaci, A. Harries, *Treatment of tuberculosis: Guidelines for national programmes; 2nd Eds.*, 1997, 1-77.
- S. Petrella, N. Gelus-Ziental, A. Maudry, C. Laurans, R. Boudjelloul, W. Sougakoff, *PLoS One*, 2011, **6**, e15785.
- K. Konno, F. M. Feldmann, W. McDermott, *Am. Rev. Respir. Dis.*, 1967, **95**, 461.
- A. Scorpio, Y. Zhang, *Nat. Med.*, 1996, **2**, 662.
- X. Du, W. Wang, R. Kim, H. Yakota, H. Nguyen, S. H. Kim, *Biochem.*, 2001, **40**, 14166.
- N. Lemaitre, I. Callebaut, F. Frenois, V. Jarlier, W. Sougakoff, *Biochem. J.*, 2001, **353**, 453.
- M. Gallo, A. Favila, D. Glossman-Mitnik, *Chem. Phys. Lett.*, 2007, **447**, 105.
- N. Saikia, R. C. Deka, *Chem. Phys. Lett.*, 2010, **500**, 65.
- N. Saikia, R. C. Deka, *Int. J. Quant. Chem.*, 2013, **113**, 1272.
- N. Saikia, S. K. Pati, R. C. Deka, *Appl. Nanosci.*, 2012, **2**, 389.
- N. Saikia, A. N. Jha, R. C. Deka, *J. Phys. Chem. Lett.*, 2013, **4**, 4126.
- G. Zuo, X. Zhou, Q. Huang, H. Fang, R. Zhou, *J. Phys. Chem. C*, 2011, **115**, 23323.
- Y. Wang, Z. Li, J. Wang, J. Li, Y. Lin, *Trends Biotechnol.*, 2011, **29**, 205.
- Y. Zhang, C. Wu, S. Guo, J. Zhang, *Nanotechnol. Rev.*, 2013, **2**, 27.
- S. K. Kirkpatrick, C. D. Jr. Gelatt, M. P. Vecchi, *Science*, 1983, **220**, 671.
- D. S. Goodsell, A. J. Olson, *Proteins*, 1990, **8**, 195.
- D. R. Westhead, D. E. Clark, C. W. Murray, *J. Comput. Aided Mol. Des.* 1997, **11**, 209.
- G. Jones, P. Willett, R. C. Glen, A. R. Leach, R. Taylor, *J. Mol. Biol.* 1997, **267**, 727.
- R. Thomsen, M. H. Christensen, *J. Med. Chem.*, 2006, **49**, 3315.
- D. K. Gehlhaar, G. Verkhivker, P. A. Rejto, D. B. Fogel, L. J. Fogel, S. T. Freer, *Proceedings of the Fourth International Conference on Evolutionary Programming*, 1995, 615.
- S.-Y. Huang, S. Z. Grinter, X. Zou, *Phys. Chem. Chem. Phys.*, 2010, **12**, 12899.
- N. Saikia, A. N. Jha, R. C. Deka, *RSC Adv.*, 2013, **3**, 15102.
- E. F. F. da Cunha, T. C. Ramalho, R. C. Reynolds, *J. Biomol. Struct. Dyn.*, 2008, **25**, 377.
- G. M. Morris, D. S. Goodsell, R. S. Halliday, R. Huey, W. E. Hart, R. K. Belew, A. J. Olson, *J. Comput. Chem.*, 1998, **19**, 1639.
- <http://molegro.com/mvd-product.php>.
- B. D. Bursulaya, M. Totrov, R. Abagyan, C. L. Brooks, *J. Comput. Aided Mol. Des.*, 2003, **17**, 755.
- E. F. Pettersen, T. D. Goddard, C. C. Huang, G. S. Couch, D. M. Greenblatt, E. C. Meng, T. E. Ferrin, *J. Comput. Chem.*, 2004, **25**, 1605.
- D. van der Spoel, E. Lindahl, B. Hess, G. Groenhof, A. E. Mark, H. J. C. Berendsen, *J. Comput. Chem.*, 2005, **26**, 1701.
- H. J. C. Berendsen, J. P. M. Postma, W. F. van Gunsteren, A. DiNola, J. R. Haak, *J. Chem. Phys.*, 1984, **81**, 3684.
- W. Humphrey, A. Dalke, K. Schulten, *J. Mol. Graphics*, 1996, **14**, 33.
- The PyMOL Molecular Graphics System, Version 1.5.0.4 Schrödinger, LLC.
- A. Fasolino, J. H. Los, M. I. Katsnelson, *Nat. Mater.*, 2007, **6**, 858.
- C. Lv, Q. Xue, D. Xia, M. Ma, J. Xie, H. Chen, *J. Phys. Chem. C* 2010, **114**, 6588.
- A. N. Unissa, N. Selvakumar, S. Hassan, *Bioinformatics*, 2009, **4**, 24.
- H. Zhang, J. Y. Deng, L.-J. Bi, Y.-F. Zhou, Z.-P. Zhang, C.-G. Zhang, Y. Zhang, X.-E. Zhang, *FEBS J.*, 2008, **275**, 753.
- N. Saikia, S. Rajkhowa, R. C. Deka, *J. Comput. Aided. Mol. Des.*, 2013, **27**, 257.
- J. H. Los, M. I. Katsnelson, V. Yazyev, K. V. Zakharchenko, A. Fasolino, *Phys. Rev. B*, 2009, **80**, 121405.

TABLE OF CONTENTS

Graphene nanomaterial can open up future perspective as suitable delivery payloads for pyrazinamide antitubercular drug targeting onto pncA protein